UNIVERSITY OF MINNESOTA
ST. ANTHONY FALLS HYDRAULIC LABORATORY
LORENZ G. STRAUB, Director

Technical Paper No. 14, Series B

Importance of Secondary Flow in Guide Vane Bends

Limited Distribution of Paper Presented Before
The Third Midwestern Conference on Fluid Mechanics at the University of Minnesota,
Minneapolis, Minnesota, March 23, 24, and 25, 1953

by

EDWARD SILBERMAN

January, 1953
Minneapolis, Minnesota

A B S T R A C T

For purposes of analysis, the flow in a guide vane bend is divided into a basic or primary two-dimensional flow with superimposed secondary flow. The two-dimensional flow is reviewed briefly first. It is then shown from experimental data that, for practical purposes, the secondary flow has negligible influence on the two-dimensional deflection, but the two-dimensional head loss is increased materially by the secondary flow. The effect of the secondary flow on head loss can be divided into two parts. The first part causes a loss which can be measured immediately behind the vanes, while the second part causes a loss which occurs between the trailing edges of the vanes and a plane about 4 duct hydraulic diameters behind the miter line of the bend. The second part is considerably larger than the first and may be attributed to increased wall shear downstream of the vanes. The increased wall shear is, in turn, attributable to the redistribution of streamlines by the secondary flow.

C O N T E N T S

LIST OF ILLUSTRATIONS

IMPORTANCE OF SECONDARY FLOW IN GUIDE VANE BENDS

I. INTRODUCTION

Research on diversion of incompressible fluid flows has been conducted at the St. Anthony Falls Hydraulic Laboratory over a period of seven years. A general conclusion from the research is that the streamlines in flow diversion problems tend to follow the potential flow pattern which is uniquely associated with the boundaries. If the velocity profile at the beginning of the diversion were irrotational, the flow would be nearly potential (allowing for boundary layer development). Because the entrance velocity profile is generally rotational, the potential streamlines have superimposed upon them a secondary flow which sometimes entirely masks the primary, nearly potential flow. The potential flow may be looked upon as a first approximation and the potential flow plus approximate secondary flow as a second approximation to the real flow in a flow diversion problem.

This paper presents a demonstration and application of the concept of separable primary flow and superimposed secondary flow to incompressible flow in a guide vane bend. The paper is based on research sponsored by the Office of Naval Research and is condensed from a technical report prepared for that organization [1]*. Squire and Winter [2], among others, have considered the same subject in a similar manner; their paper shows the theoretical development of the secondary currents using the Helmholtz form of the equations of motion but does not describe the complete role of the secondary currents and their influence on the primary flow.

This paper is specifically concerned with fixed, two-dimensional guide vane structures like those shown in the installation in Fig. 1. However, the results are at least qualitatively applicable to all types of blading installations. Figure 2 is a photograph of a set of guide vanes installed in a 90° test bend used in the present experimental work. A survey for total head and flow direction behind the vanes is in progress using a pitot cylinder.

Figure 3 contains typical experimental results. Plotted in Fig. 3b are total head distribution and flow direction immediately behind the vanes,

---

*Numbers in brackets refer to references on p. 10.

while Fig. 3a shows total head distribution in a straight duct under the same entrance conditions as those shown in Fig. 3b. Figure 3d locates the survey planes. Figure 3c shows the results of a survey taken at a station designated M-M and located just over 4 hydraulic diameters downstream of the miter line of the bend; it is seen that the total head distribution here is roughly similar to that in the straight duct. From this and other evidence, it was concluded that the influence of the bend was complete, for practical purposes, in the present experiments at station M-M or before.

Examination of Fig. 3b shows that there is a large, two-dimensional, nearly potential flow region surrounding the horizontal center line of the duct, marred only by the wakes of the vanes. There is another region near the vane ends which is disturbed by secondary flows. Perhaps the two-dimensional region is better illustrated in Fig. 4, which is a plot of head loss in a plane at midspan behind the vanes and shows even more clearly the nearly potential character of the two-dimensional flow. (Figure 4 is for a type of vane different from that shown in Fig. 3, but the results are typical.)

These experimental results led naturally to the question, how much different would Fig. 3c appear if a purely two-dimensional flow through the vanes were considered? That is, what difference is there between the real flow and the two-dimensional flow used as a first approximation?

II. TWO-DIMENSIONAL FLOW

To answer the questions just posed, it is necessary to look at the two-dimensional flow first. The two-dimensional flow through a cascade of vanes may be obtained theoretically by one of several methods [3, 4] or by experiment. If theoretical methods are used, the boundary layers on the vanes must be taken into account separately [5]. In the present work, the two-dimensional flow was obtained experimentally.

The terms used in defining a two-dimensional cascade of guide vanes are illustrated in Fig. 5. Each vane in the cascade develops a reaction or lift which changes the momentum of the flow from the old direction to the new direction. The coefficients of lift and drag C_L and C_D, and the line of action of the lift making the angle γ with the cascade axes are related to

the deflection angle Δ, the velocity ratio V_2/V_1, the entrance angle β_1, the exit angle β_2, and the spacing-chord ratio s/c through the equations of continuity, momentum, and energy. These relations are given by the equations

$$\frac{C_L}{s/c} = 2 \frac{V_2}{V_1} \frac{\sin\Delta}{\cos\gamma} - \frac{C_D}{s/c} \tan\gamma \tag{1}$$

$$\tan\gamma = \frac{1}{2} (\cot\beta_2 + \cot\beta_1) \tag{2}$$

and are plotted in Fig. 6 with $C_D = 0$ (C_L and C_D are based on the entrance velocity head $V_1^2/2g$). This figure shows, for example, that each vane in a two-dimensional cascade installed in a 90° miter bend ($\Delta = 90^\circ$, $V_2/V_1 = 1.0$) must be capable of developing a lift coefficient of 2 s/c. Whether or not a vane will develop such a coefficient depends on its shape (principally camber), its stagger angle θ, its spacing-chord ratio in the cascade s/c, and the entrance angle β_1 or exit angle β_2.

It is shown in the basic technical report [1] that given a cascade defined by the profiles of its vanes, their stagger angle θ, and spacing-chord ratio s/c, the approximate relation

$$\cot\beta_2 = A \cot\beta_1 - B \tag{3}$$

exists where A and B are constants for the given cascade. Equation (3) plots as a straight line on Fig. 6. In Fig. 7, several such cascade lines are taken from experimental data by Davis [6] and Harris and Fairthorne [7] and are plotted to the same coordinates as Fig. 6. The Harris and Fairthorne data are all for the same vane profile, θ and s/c being varied. The cascade lines are of limited length because the vanes stall when the entrance angle is too small or too large and then Eq. (3) no longer holds. If each vane could be operated as a single airfoil, without stalling, it would have an angle of attack at zero lift of α_o. It is also shown in the basic reference [1] that a cascade line should pass through the value

$$\beta_o = \beta_1 = \beta_2 = \theta - \alpha_o \tag{4}$$

Harris and Fairthorne measured their value of α_o as -11.5°, and the cascade lines in Fig. 7 representing their data have been drawn to pass through the corresponding value of β_o.

If cascade lines were available to cover the entire Fig. 7, together with drag coefficient values, two-dimensional data could be taken from that figure without resort to theoretical computation or experiment. Such lines are not available, however.

The present experimental work was confined to three vane profiles which were used in cascade to produce $\Delta = 90^\circ$, $V_2/V_1 = 1.0$. Two-dimensional data were obtained in the midspan region of vanes of 9-in. span and 2.02-in. to 4.25-in. chord. The vane profiles are shown in Fig. 8. Figure 9 shows the stagger angle required for each cascade and Fig. 10a the corresponding head loss coefficient ζ_2 where

$$\text{Head Loss} = \zeta_2 \frac{V_1^2}{2g} \tag{5}$$

The head loss was measured experimentally by determining the average total head behind the vanes and at the corresponding position in a straight duct. The loss is the difference between these values. In Fig. 10b, the drag coefficient for each cascade is shown. For the present conditions

$$C_{D_2} = \zeta_2 \frac{s}{c} \tag{6}$$

The Reynolds number for all data is $V_1 c/\nu = 1.5 \times 10^5$ where ν is the kinematic viscosity. The vanes are smooth brass or aluminum. There was some indication of change in head loss coefficient, but there was no measurable change in deflection in the range of Reynolds number from about 0.5 to 4.0×10^5. (Since $C_L = 2\ s/c$ for the present experiments, Fig. 9 corresponds to the angle of attack versus lift coefficient, Fig. 10a to the lift-drag ratio versus lift coefficient, and Fig. 10b to the coefficient of drag versus lift coefficient curves of single airfoil theory.)

III. SECONDARY FLOW

The data of Fig. 9 are not truly two-dimensional. In obtaining these data, the stagger angle was adjusted for each cascade until it appeared that the cascade alone was turning the fluid (without assistance from the walls). Correct stagger angle was obtained when the pressure was uniform across the duct upstream of the vanes and the pressures at corresponding points in the two-dimensional region on several vane surfaces were equal. Determinations of stagger angle were made over a range of chord aspect ratios (AR_c = span over chord) from about 1 to 4.5 and of space aspect ratios (AR_s = span over space) from about 2 to 9. The range of aspect ratios was obtained by using vanes of different chord length at constant span and spacing-chord ratio, and vanes of two different spans at constant chord length and spacing-chord ratio. There was no measurable change in required stagger angle due to these variations, whereas there was a change in head loss. It was therefore concluded that the average deflections were independent of aspect ratio and must have been identical with the two-dimensional deflection for each cascade.

In Fig. 11, three-dimensional head loss coefficients are plotted against spacing-chord ratio. Three groups of data are shown. The lower pair of curves on each graph represent two-dimensional values taken from Fig. 10a. The curves are obtained by integrating the two-dimensional head loss over the approach velocity profile; one over the vane span and one vane space, and the other over the entire duct cross section. If there were no secondary flow influence on the two-dimensional drag, these curves should also represent the experimental three-dimensional head loss.

The remaining curves and data-points show the trend of the three-dimensional experimental data. The ζ_3 curve represents the head loss data obtained from measurements at 0.5 chord length behind the vane trailing edges and taken over one vane span and one vane space. The nearby points marked ζ_b are similar but are obtained from measurements taken over the entire duct cross section. These data lie, on the average, some 30 per cent above the corresponding integrated two-dimensional curves. The increase in loss is not very large, but does exist. The differences between the ζ_b and ζ_3 points represent the experimental effect of the lateral duct walls. The differences are seen to be very small for the data shown (of the order of 0.01 or 0.02 $V_1^2/2g$), but when the number of vanes in the duct was reduced to 4 or 5, ζ_b increased greatly.

The upper group of curves and data-points in Fig. 11, marked ζ_m, represent the head loss coefficients obtained from measurements further downstream. These were taken at station M-M where the rate of loss was approximately the same as in the straight duct. The data-points fall 100 per cent and more above the integrated two-dimensional curves and also well above the ζ_3 and ζ_b curves. The data scatter, but much of the scatter is eliminated by grouping the points by chord length (there was no variation of ζ_2 with chord length). The remaining scatter may be attributed to experimental error (the estimated accuracy of the measurements of average total head is 2 per cent of the dynamic head, and since the head loss is the difference between two average total heads, the possible error is 4 per cent) and to the use of three different shapes of duct with somewhat different entrance velocity profiles. The head loss represented by the difference in ζ_m and ζ_b points must occur downstream of the vanes.

Since it appears that the excess head loss in a guide vane bend is associated with the secondary flow, it is desirable to relate the two by computation. Squire and Winter [2] and the basic reference [1] show that just beyond the beginning of curvature, the vorticity component ξ parallel to the two-dimensional streamlines is given by

$$\xi = 2\epsilon\eta_o \tag{7}$$

where ϵ is the small angle through which each streamline has turned and η_o is the vorticity component normal to the streamlines and vane spans at the beginning of curvature. Squire and Winter have extended Eq. (7) to the entire bend by taking ϵ as the total turning angle of the two-dimensional streamlines and η as constant both along the streamlines and parallel to the vane spans. This ignores any influence of the secondary flow on the basic two-dimensional motion. Having computed the resulting secondary flow on this basis, they arbitrarily take the energy loss as half the kinetic energy of the secondary flow. It is believed that the Squire and Winter assumptions beyond Eq. (7) cannot be used to obtain quantitative data and that the true nature of the secondary flow is obscured by those assumptions.

Generally, the vorticity η_o is very large near the duct walls and decreases rapidly toward the interior of the fluid. After a small increment of turning ϵ, the vorticity components ξ will be roughly as sketched in Fig. 12a; the size of each vortex figure indicates the relative strength of the vorticity. The associated velocity pattern will be like that sketched in Fig. 12b. At succeeding sections around the bend, η_o takes on different values and ξ will vary; but, qualitatively, these sketches still give a picture of what must occur. The flow pattern of Fig. 12 has been confirmed in experimental observations and photographs of yarns and wall coatings. It has also been observed by others; some excellent photographs were published recently by the National Advisory Committee for Aeronautics [8]. At the trailing edge of each vane, two vertical currents meet and form a vortex sheet; this is identical with the sheet which would be attributed to the decrease in circulation near the span ends. There is no further vorticity ξ developed beyond the trailing edges, but the flow in the boundary layer continues toward the inside wall and along that wall toward its center.

The important consequence of the preceding discussion is not so much that a secondary flow develops, but rather that this secondary flow behaves in such a way that it carries low-energy fluid from the duct boundary layer down the suction surface of each vane into the interior of the fluid, and high-energy fluid from the interior to the duct wall. This redistribution of the streamlines is observable in the total head surveys plotted in Fig. 3b. The streamlines are indicated schematically in Fig. 13. Here A-A represents the two-dimensional streamlines in the interior, B the separation region associated with the two-dimensional boundary layer, C-C the upstream boundary layer streamlines, and C'-C' the streamlines originally in the interior which are carried to the boundary by the secondary flow.

The strength of the secondary flow depends on the ratio $C_L/(s/c)$ of the two-dimensional flow (Fig. 6), the profiles of the vanes, and the entrance velocity profile; there may be other minor factors. The present data did not permit study of these factors; a recent publication of the National Advisory Committee for Aeronautics [8] gives some data on the first factor.

The relation between the excess head loss and the secondary flow is now apparent. In Fig. 11, the difference between ζ_3 and ζ_2, the excess loss at the vanes, is associated with the development of the trailing vortices and also with the modification of the two-dimensional boundary layer flow at the

vane surfaces. That is, where separation occurs at the vane surface in the two-dimensional region, it may not occur near the span ends. The difference between ζ_m and ζ_b, the excess loss downstream of the vanes, is associated with increased friction at the duct wall where high-energy, high-velocity fluid now forms the boundary layer.

The part of the loss occurring at the vanes is comparatively small, and not too much attention has been given to it yet. Carter and Cohen [9] have computed the part of the drag coefficient attributable to the trailing vortices within an unknown factor representing the distance between each rolled-up trailing vortex and the duct wall. Because of this unknown factor, their computation cannot be verified directly using the present data.

A rough computation of the loss coefficient attributable to additional shear at the wall was made in the basic reference. The formula was obtained

$$\zeta_\tau = 0.03 \, \overline{K} \, \frac{s x_2}{s \ell} \tag{8}$$

where ζ_τ is the head loss coefficient attributable to the greater shear at the wall,

$\overline{K}$ is a parameter depending on entrance velocity profile ($\overline{K} \approx 1/3$ for the present experiments), and

$\frac{s x_2}{s \ell}$ is half the ratio of wall area experiencing additional shear to passage area between the vanes.

In the formula, x_2 is the distance required downstream of the vanes for the disturbed velocity profile to return approximately to its value at the entrance to the vanes. The experiments indicated that x_2 tended to increase with decreasing spacing between the vanes for the plate vanes but was more nearly constant for the thick vanes. Assuming that at the closest vane spacing in the present experiments (about 1 in.) the boundary layer did not return to normal until station M-M was reached ($x_2 \approx 30$ in.), Eq. (8) yielded

$$\zeta_\tau = \frac{0.3}{s \ell} \tag{8a}$$

where $s \ell$ is the passage area in square inches.

In Fig. 14, experimental values of $\zeta_m - \zeta_2$ have been plotted against $1/s\ell$ for one of the plate vanes, and Eq. (8a) for ζ_τ is also shown. It is to be remembered that the values of $\zeta_m - \zeta_2$ include not only ζ_τ but also the coefficients of the losses occurring at the vanes and in the spaces between the vanes and walls (of the order of 0.05). The trend of the data follows the formula. Other data show that at the largest passage areas (where there were too few vanes in the bend), the trend of the data was opposite to that of the formula.

The thick vanes used in these experiments were designed with constant gap between the vanes; x_2 was more nearly constant than for the plate vanes, so that Eq. (8) indicates that ζ_τ should tend to remain constant. The experimental values of $\zeta_m - \zeta_2$ for these vanes were also roughly constant.

In conclusion, it has been shown that the secondary flows increase the two-dimensional loss coefficient, principally by increasing the wall shear downstream of the vanes but also by increasing the loss at the vanes. The head loss coefficient ζ in a guide vane bend may be written

$$\zeta = \zeta_2 + \zeta_i + \zeta_\tau \tag{9}$$

where ζ_2 is the two-dimensional loss coefficient,
ζ_i is the loss coefficient at the vanes, and
ζ_τ is the loss coefficient, due principally to increased wall shear, downstream from the vanes.

For practical purposes, the deflection produced by a guide vane system is the same as the two-dimensional deflection.

Given $C_L/(s/c)$ for the two-dimensional flow, the vane profiles, and the entrance velocity profile, it should be possible to compute both ζ_i and ζ_τ. Methods for accomplishing this have not yet been devised.

ACKNOWLEDGMENT

This paper is based on research sponsored by the Office of Naval Research under Contract ONR-66204 and is condensed from a final report for that organization [1]. The work was performed at the St. Anthony Falls Hydraulic Laboratory under the general direction of Dr. Lorenz G. Straub, Director.

LIST OF REFERENCES

[1] Silberman, E. Secondary Flows in Guide Vane Bends With Some Notes on the Primary Two-Dimensional Flow. University of Minnesota, St. Anthony Falls Hydraulic Laboratory Project Report No. 36, January, 1953. 102 pages.

[2] Squire, H. G. and Winter, K. G. "The Secondary Flow in a Cascade of Airfoils in a Nonuniform Stream." Journal of Aeronautical Science, Vol. 18, No. 4, pp. 271-277. 1951

[3] Tyler, R. A. "The Available Theoretical Analyses of Two-Dimensional Cascade Flow." National Research Council of Canada, Aero Note, AN-4, Ottawa, 1949. 58 pages.

[4] Poritsky, H., Sells, B. E., and Danforth, C. E. "Graphical, Mechanical, and Electrical Aids for Compressible Fluid Flow." Journal of Applied Mechanics, Vol. 12, No. 1, pp. 37-46. 1950.

[5] Schlicting, H. and Scholz, N. "Theoretical Determination of Flow Losses in a Plane Cascade" (Über die Theoretische Berechnung der Strömungsverluste eines ebenen Schaufelgitter). Ingenieur-Archiv, Vol. 19, pp. 42-65. 1951.

[6] Davis, H. "A Method of Correlating Axial-Flow-Compressor Cascade Data." Transactions of the ASME, Vol. 70, pp. 951-955. 1948.

[7] Harris, R. G. and Fairthorne, R. A. "Wind Tunnel Experiments with Infinite Cascades of Airfoils." British Aeronautical Research Council, Reports and Memoranda, No. 1206. 1928.

[8] Hansen, A. G., Costello, G. R., and Herzig, H. Z. "Effect of Geometry on Secondary Flows in Blade Rows." National Advisory Committee for Aeronautics, Research Memorandum, RM E 52H26, October, 1952. 38 pages.

[9] Carter, A. D. S. and Cohen, E. "Preliminary Investigation into the Three-Dimensional Flow through a Cascade of Aerofoils." British Aeronautical Research Council, Reports and Memoranda, No. 2339. 1946.

A P P E N D I X

Figures 1 to 14

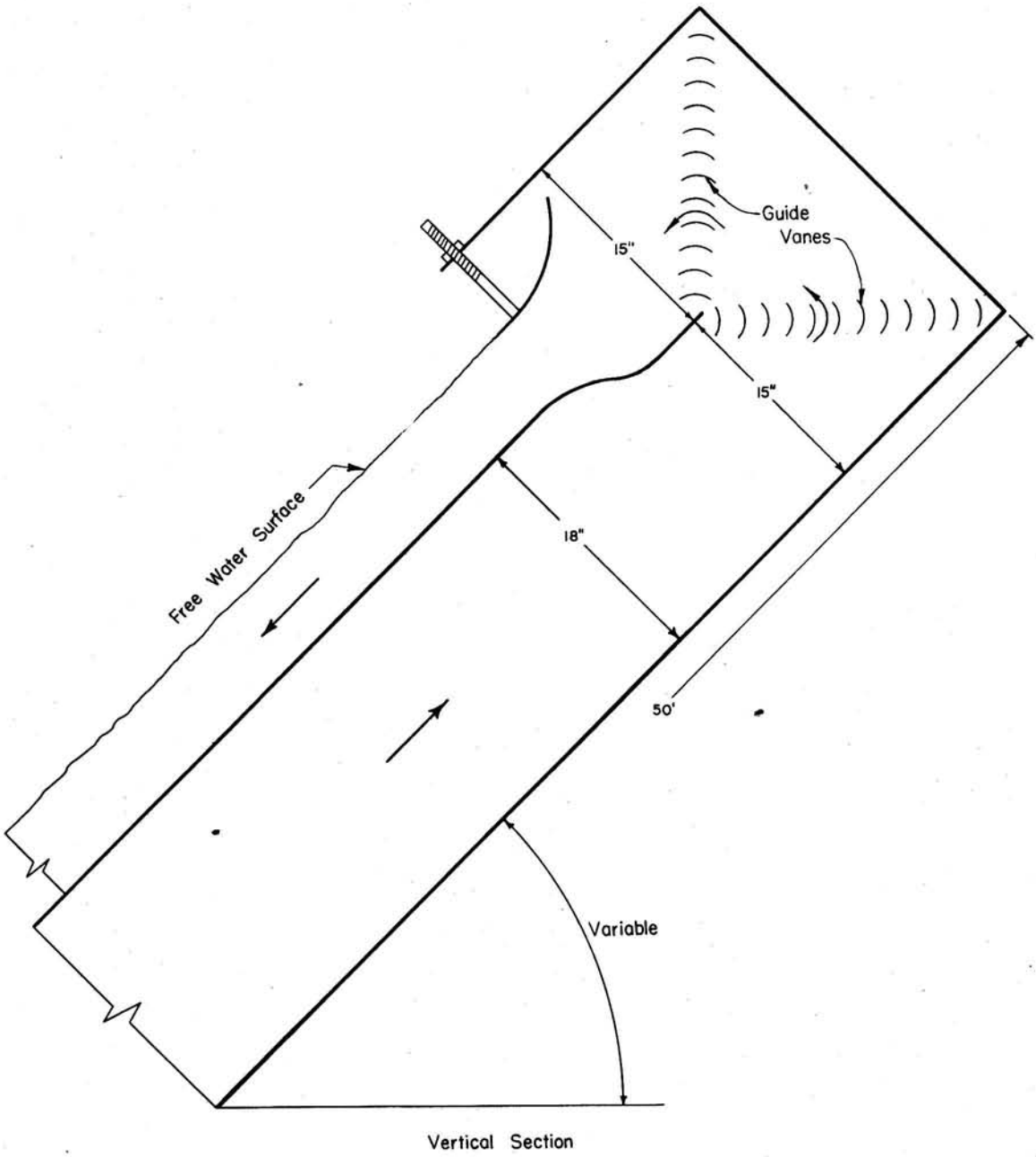

Fig. 1 - Guide Vane Installation in High-Velocity Channel

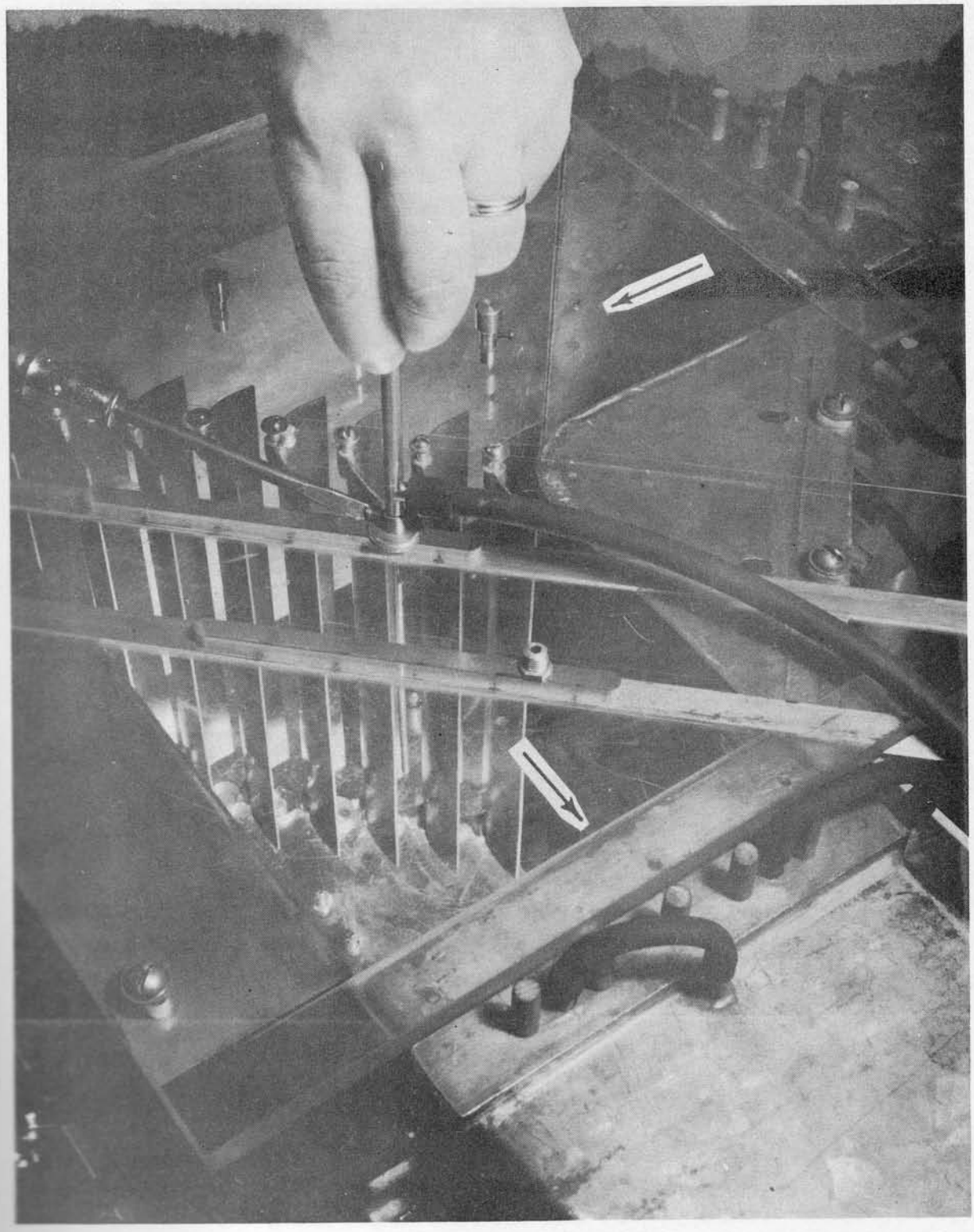

Fig. 2—Guide Vanes Installed in a Test Bend

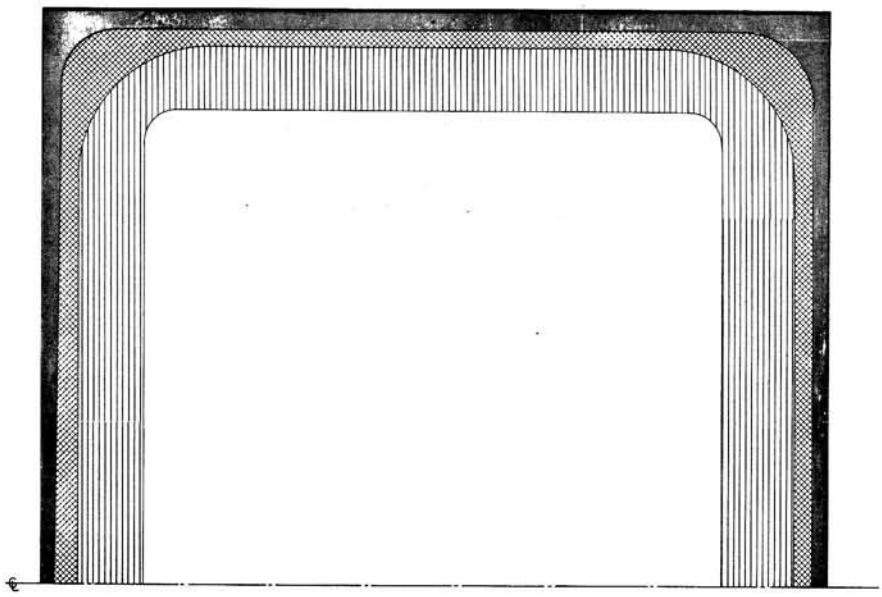

a. Straight Duct, Section A-A

Dimensionless Total Head	
	0 - 0.3
	0.3 - 0.7
	0.7 - 0.98
	0.9
	Over 0.98

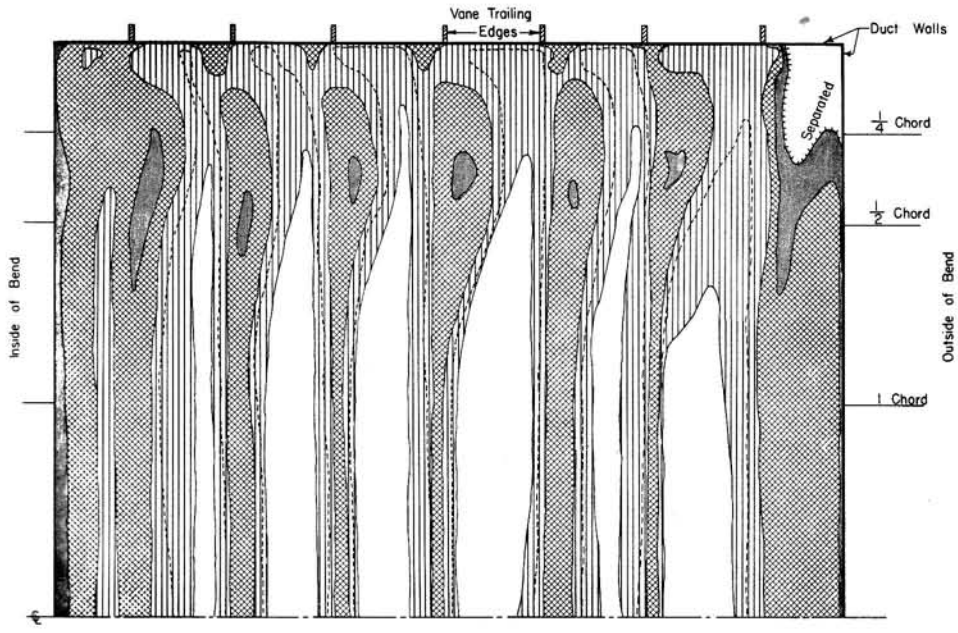

b. Immediately Downstream of Miter Elbow, Section B-B

Fig.3— Total Head Distribution in a Guide Vane Bend

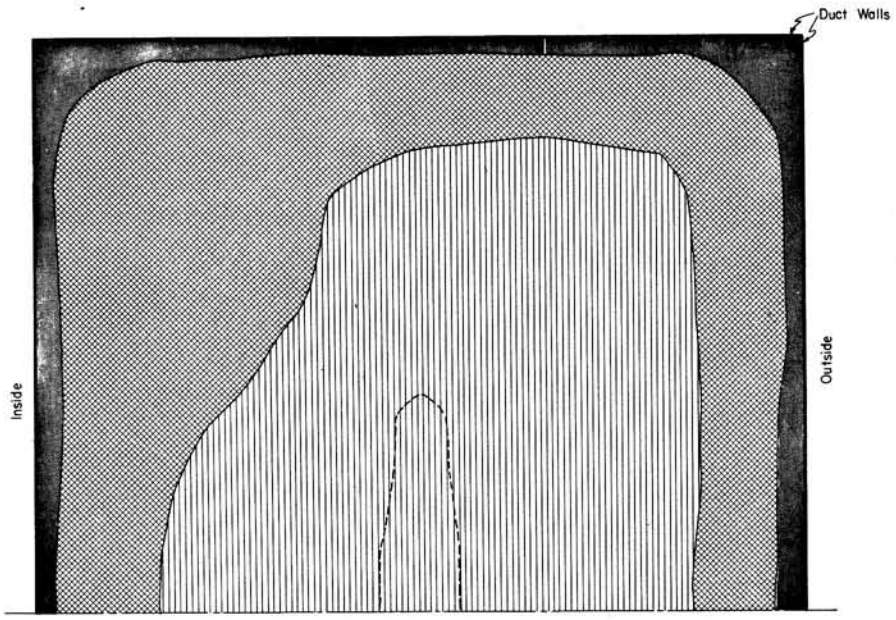

c. Downstream of Bend, Section M-M

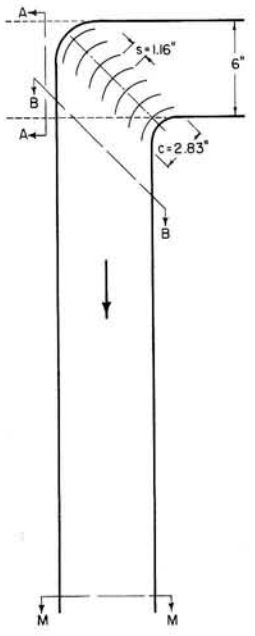

(21) 300 Vane Shape
$Re_c = 1.5 \times 10^5$
$Re_d = 3.8 \times 10^5$

d. Vane Arrangement

Dimensionless Total Head	
	0 – 0.3
	0.3 – 0.7
	0.7 – 0.98
	0.9

Fig.3– Total Head Distribution in a Guide Vane Bend

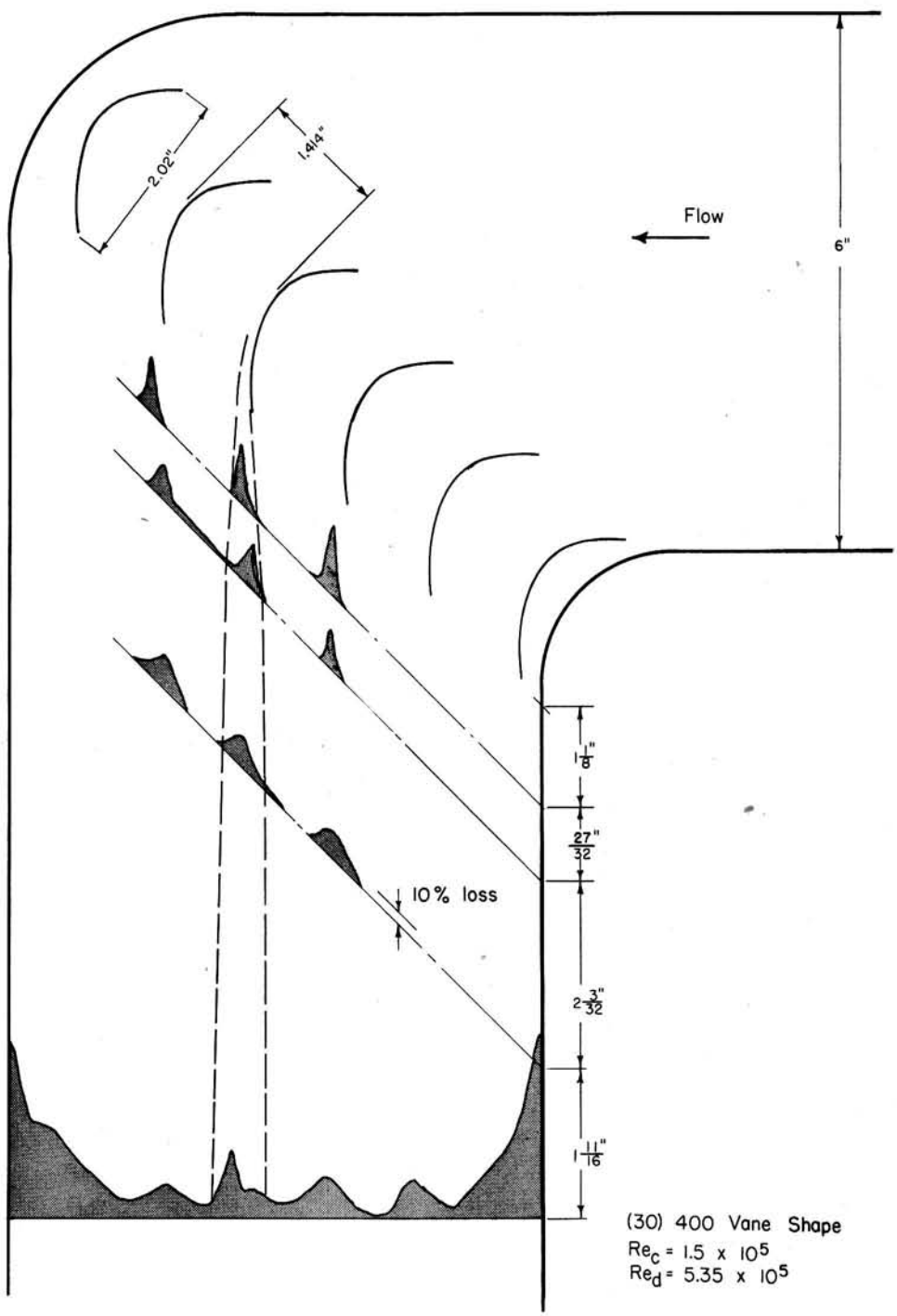

Fig. 4—Head Loss Behind the Two-Dimensional Region of a Cascade

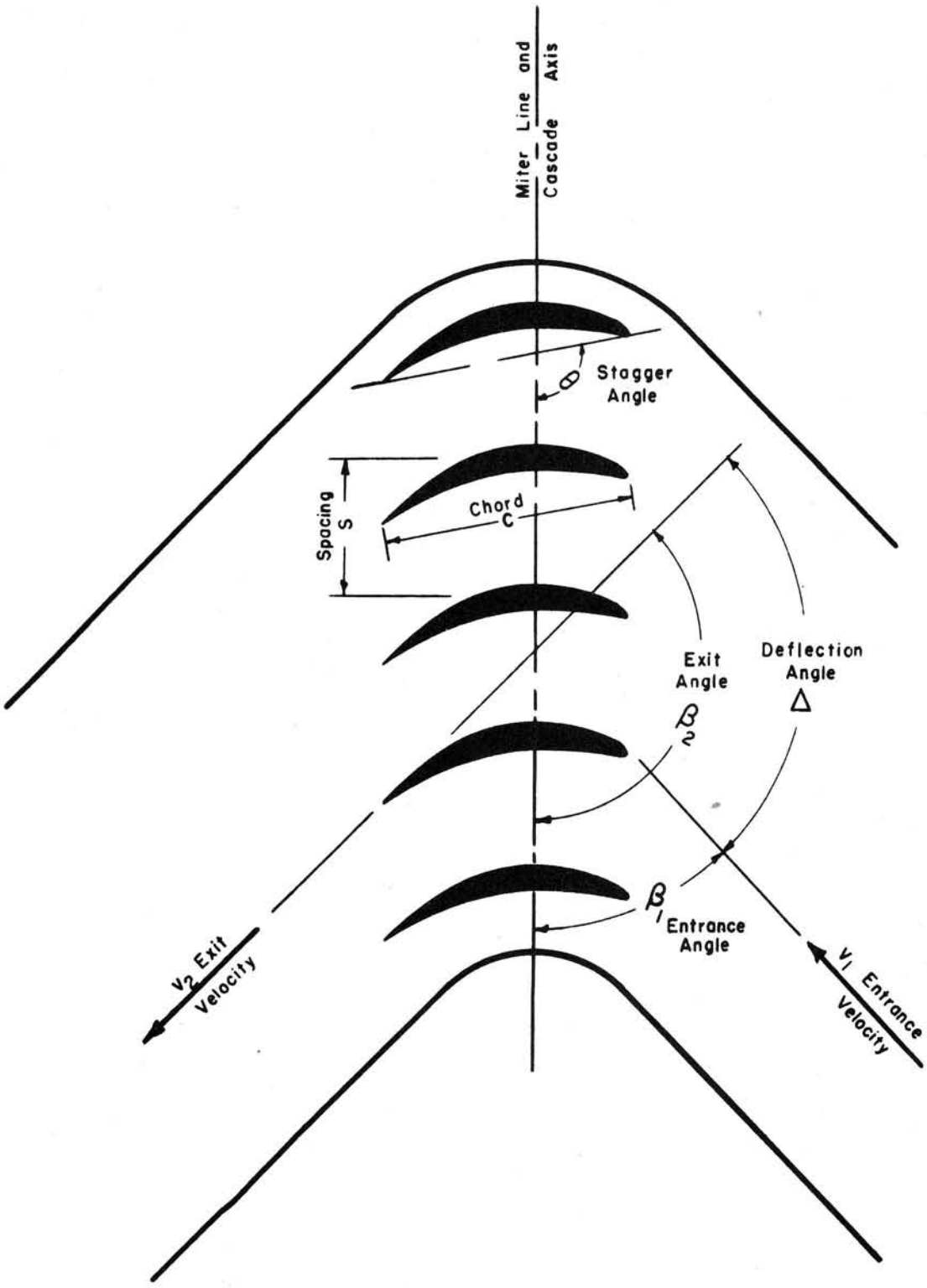

Fig.5—Cascade Characteristics

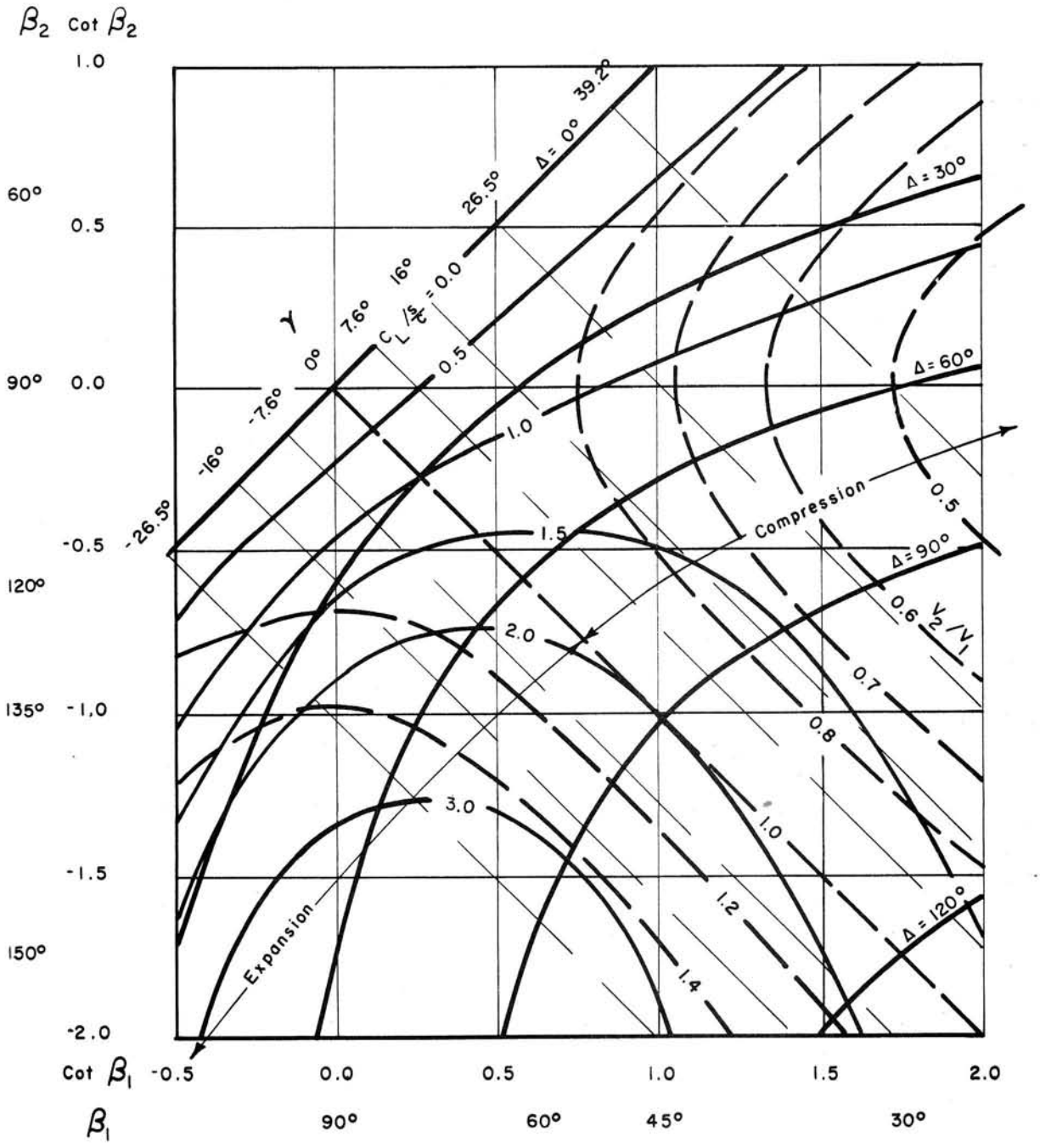

Fig.6—Relation Between Entrance and Exit Angles, Deflection Angle, and Lift Coefficient in a Cascade

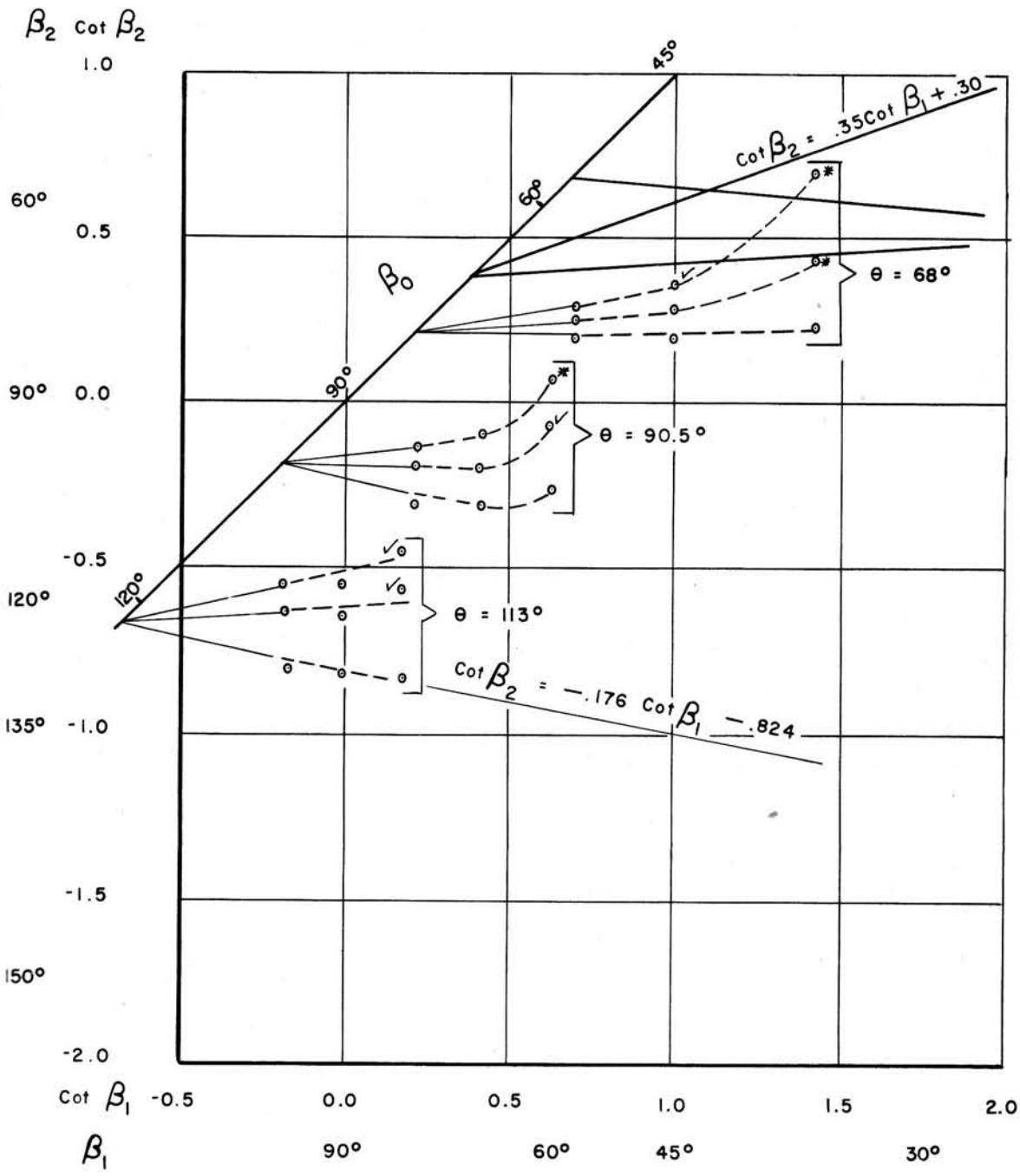

——— From Fig. 2 by Davis [6] representing experimental data
– –o– – From Harris and Fairthorne [7]

(Starred points represent stalled cascades according to reference. Checked points represent cascades with abnormally high drag.)

Fig. 7 – Typical Cascade Lines

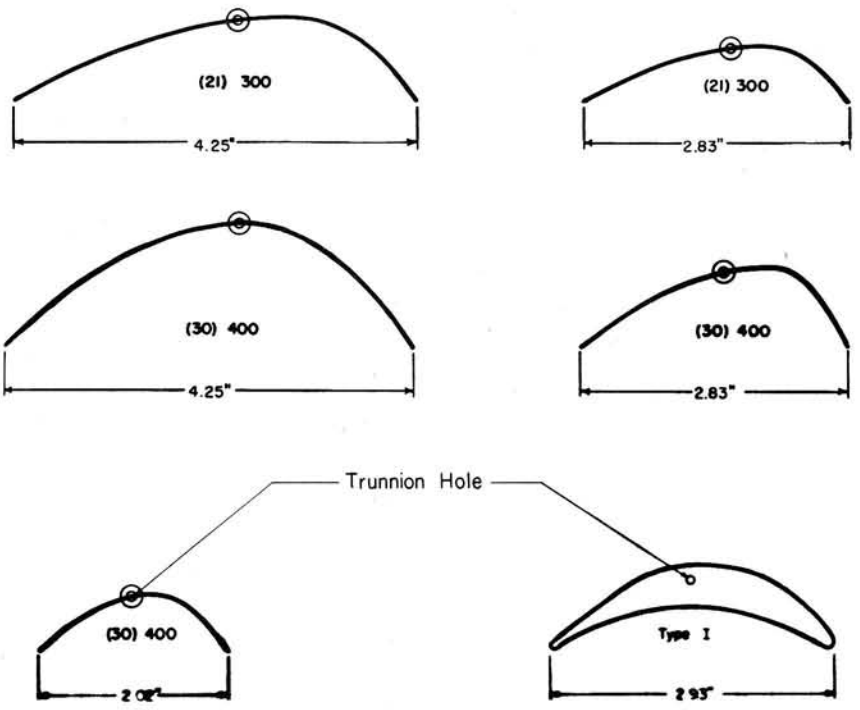

Fig. 8 – Guide Vane Profiles Used in the Experimental Work

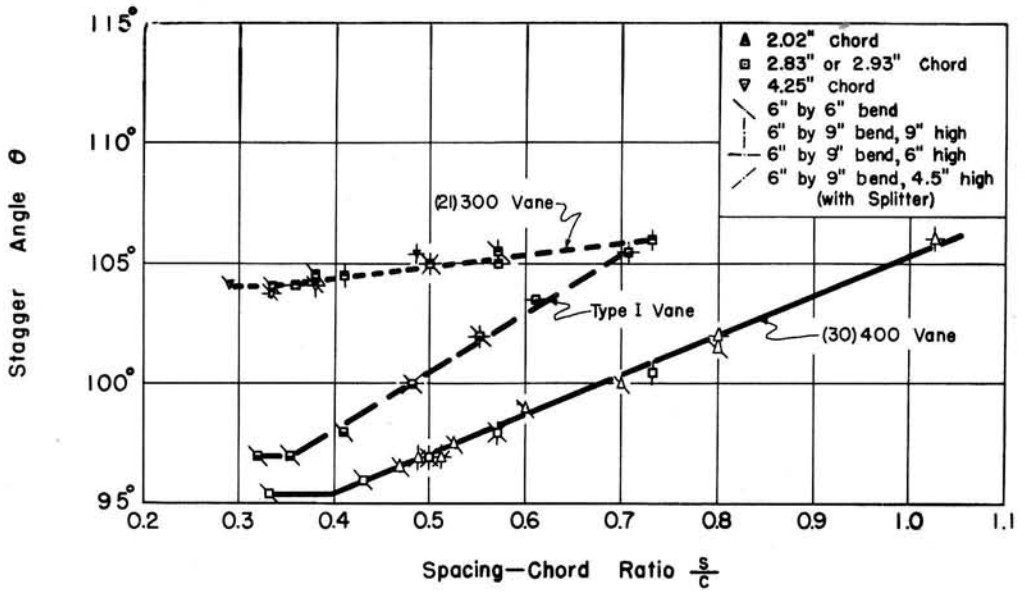

Fig. 9 – Stagger Angle Required to Produce 90° Flow Deflection

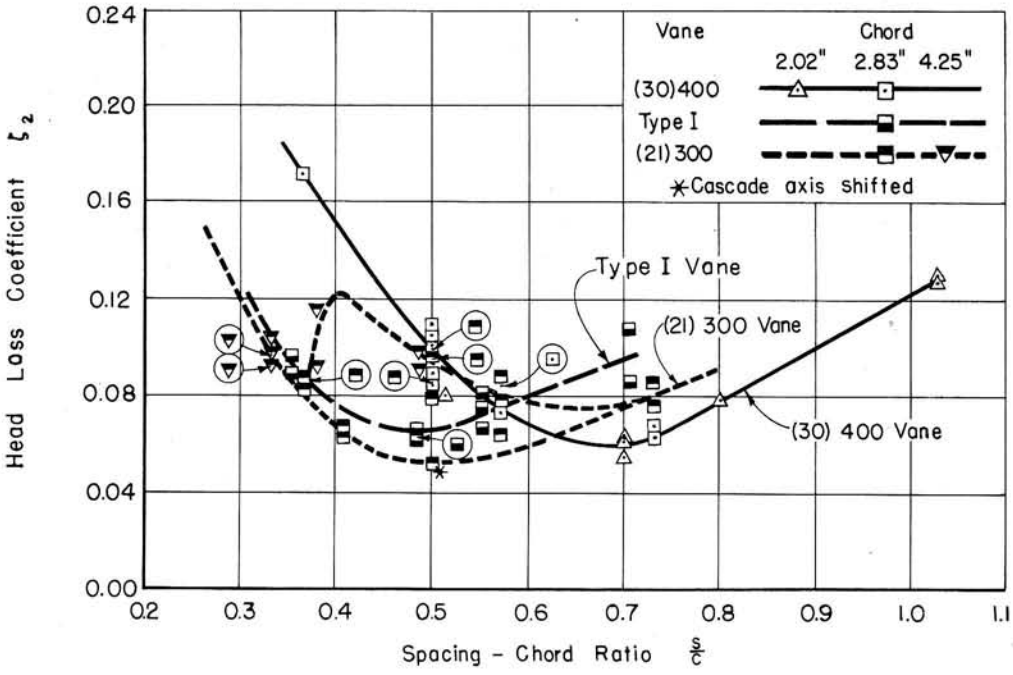

a. Head Loss Coefficient

$Re_c = 1.5 \times 10^5$

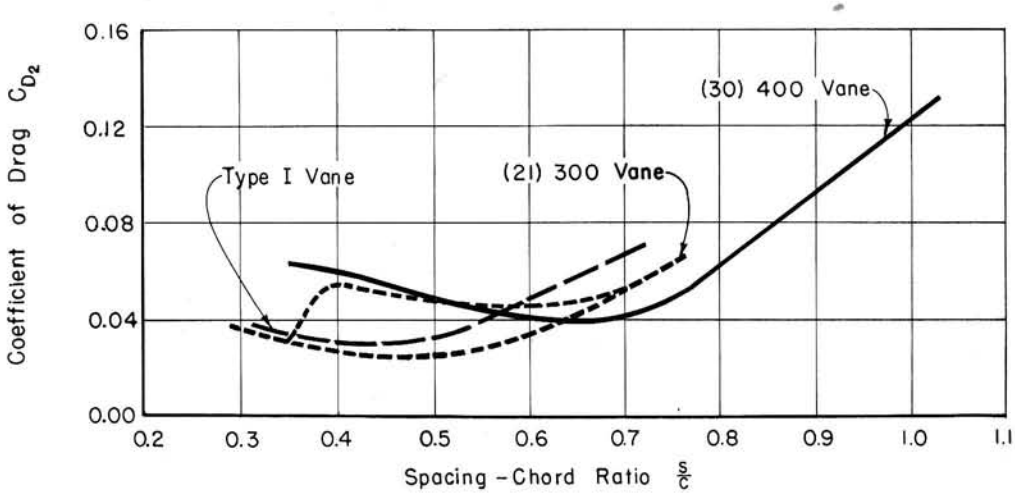

b. Coefficient of Drag

$Re_c = 1.5 \times 10^5$

Fig.10—Two-Dimensional Head Loss and Drag Coefficients

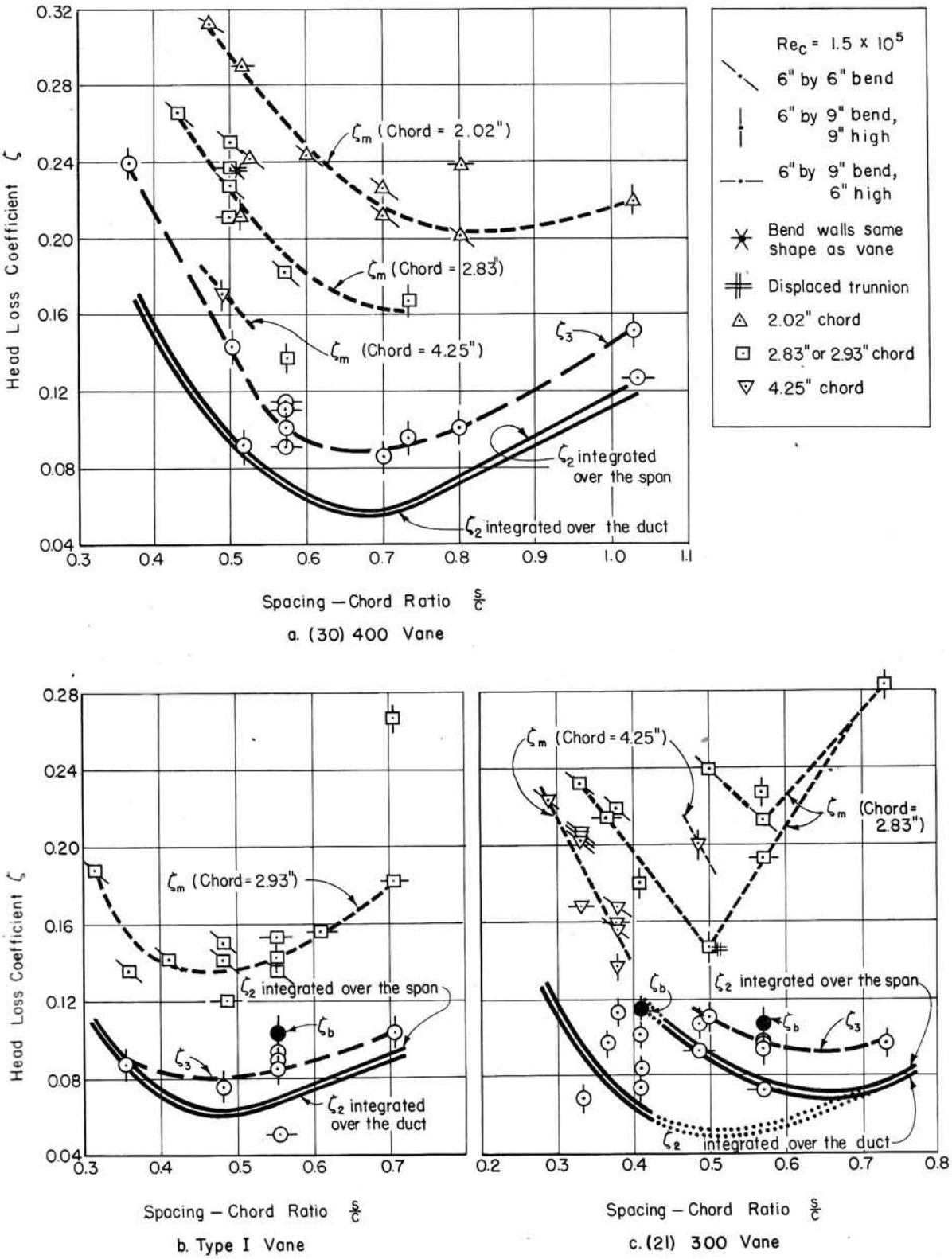

Fig. 11 — Comparison of Two-Dimensional and Three-Dimensional Head Loss Coefficients

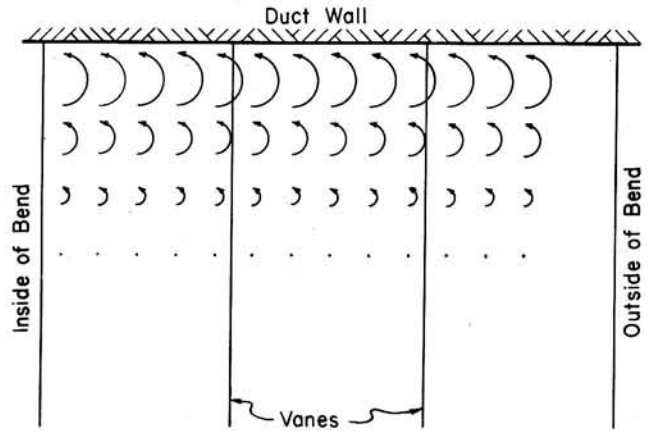

a – Schematic Vortex Distribution

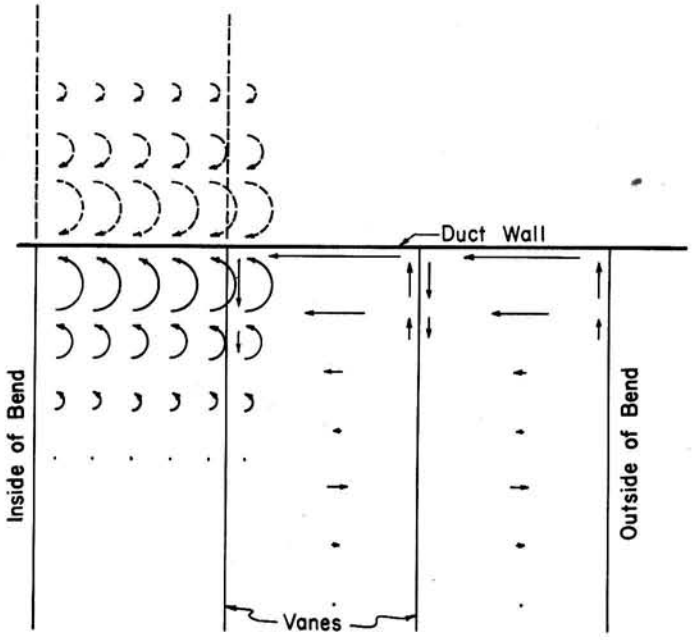

b – Schematic Secondary Flow Pattern

Fig.12 – Sketch of Secondary Flow Between the Vanes

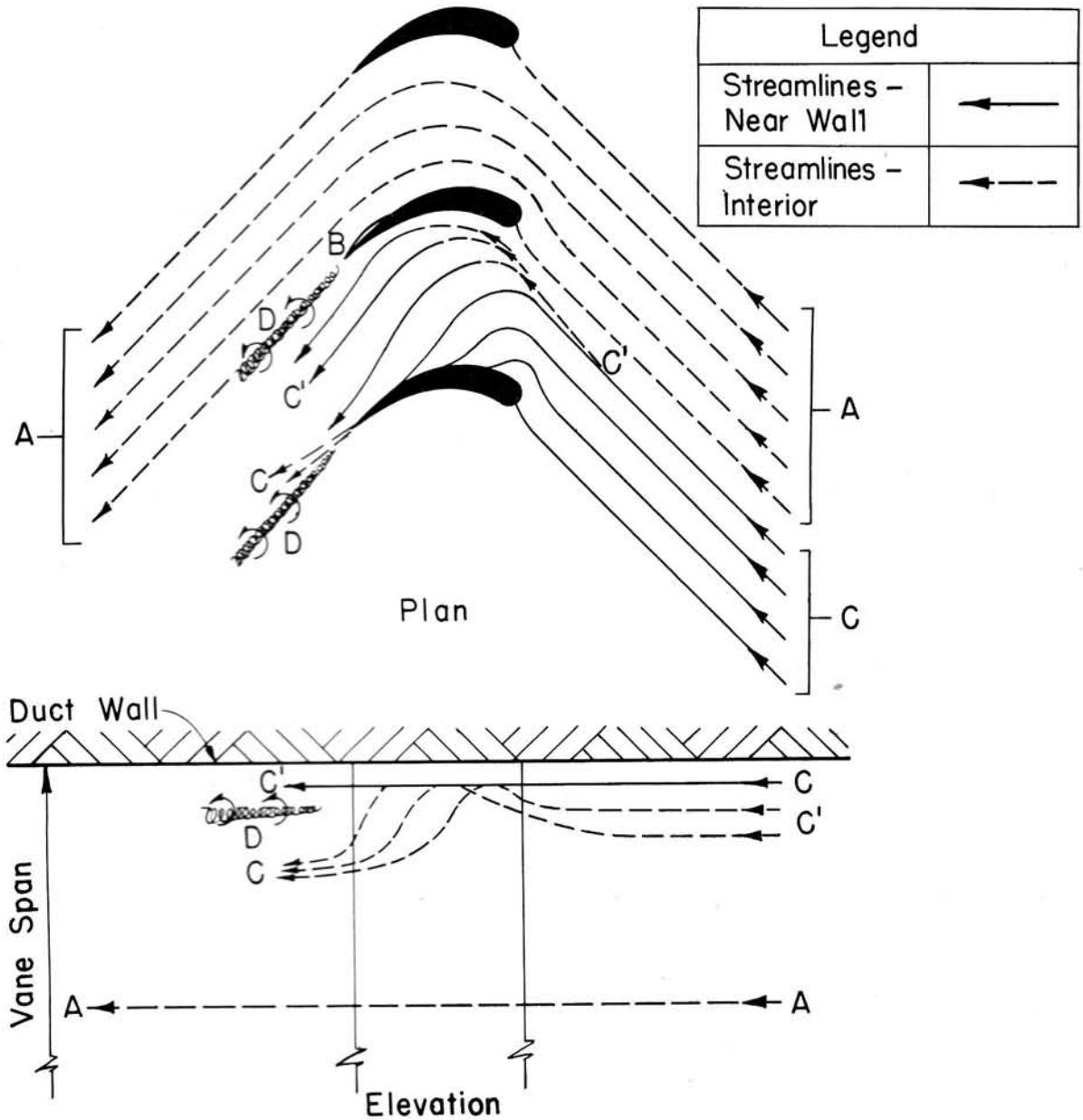

Fig.13- Schematic Streamlines in a Guide Vane Bend

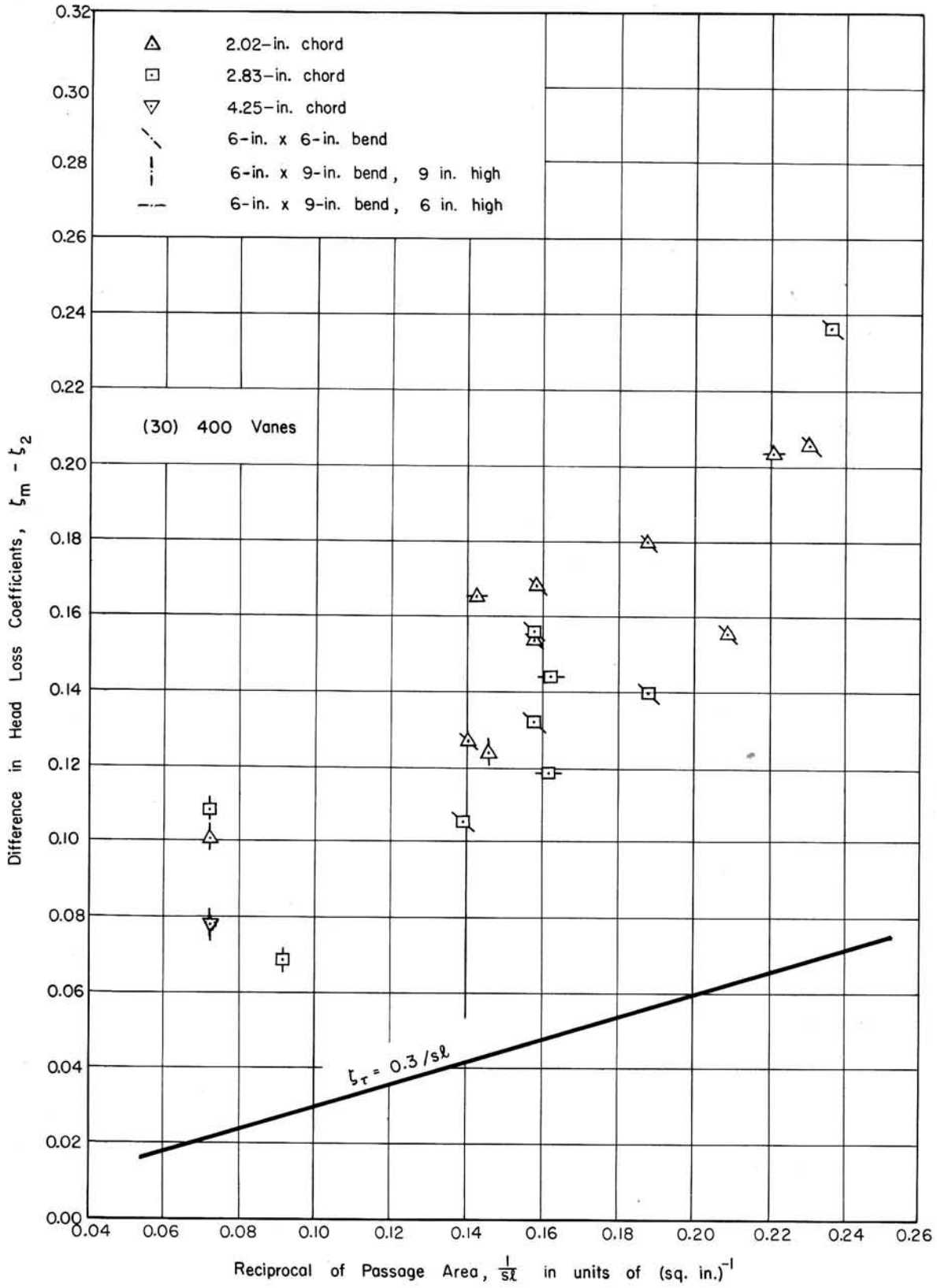

Fig.14—Comparison of Total Excess Head Loss and Computed **Loss Attributable to Wall Shear**